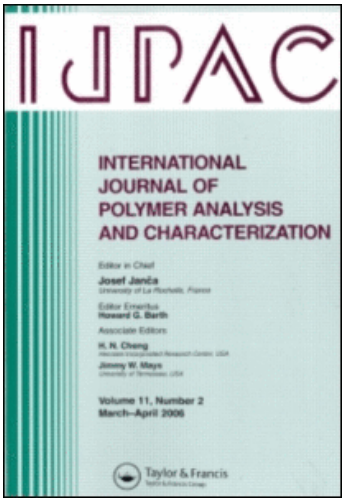

International Journal of Polymer Analysis and Characterization
Publication details, including instructions for authors and subscription information:
http://www.informaworld.com/smpp/title~content=t713646643

A New Holographic Grating Technique for the Measurement of Diffusion and Thermal Diffusion of Polymers in Solution

W. Köhler[a]; P. Rossmanith[a]
[a] Max-Planck-Institut für Polymerforschung, Mainz, Germany

To cite this Article Köhler, W. and Rossmanith, P.(1995) 'A New Holographic Grating Technique for the Measurement of Diffusion and Thermal Diffusion of Polymers in Solution', International Journal of Polymer Analysis and Characterization, 1: 1, 49 — 62
To link to this Article: DOI: 10.1080/10236669508009706
URL: http://dx.doi.org/10.1080/10236669508009706

Int. J. Polymer Analysis & Characterization
1995, Vol. 1, pp. 49–62
Reprints available directly from the publisher
Photocopying permitted by license only

A New Holographic Grating Technique for the Measurement of Diffusion and Thermal Diffusion of Polymers in Solution

W. KÖHLER,* and P. ROSSMANITH

Max-Planck-Institut für Polymerforschung, Postfach 3148, D-55021 Mainz, Germany

(Received September 26, 1993)

Despite being a fundamental transport property, thermal diffusion in polymer solutions is still poorly understood, and reliable experimental data are scarce. After a brief review of previous experimental techniques and results, the application of forced Rayleigh scattering to the study of diffusion and thermal diffusion in polymer solutions is discussed. Due to the μm diffusion lengths, equilibration times are reduced to typically 100 ms, and signal averaging allows noise reduction. From a single experiment three different diffusion coefficients are obtained without the need for chain labeling: the thermal diffusivity, the translational diffusion coefficient, and the thermal diffusion coefficient. An improved setup, allowing convection-free heterodyne detection, is discussed. Results for polystyrene in toluene and ethyl acetate are reported, and the measured translational diffusion coefficients are compared with data obtained from photon correlation spectroscopy.

KEY WORDS Polymer solution, diffusion, thermal diffusion, holography

INTRODUCTION

A temperature gradient applied to a binary solution not only causes an energy flux from the hot into the cold regions, but also gives rise to a mass flux of the solute with respect to the solvent. At least for isotropic systems, this solute flux is parallel or anti-parallel to the temperature gradient, the direction being not predictable by simple arguments.

This cross-coupling between temperature and concentration, termed *thermal diffusion* or *Ludwig-Soret effect*, was already described more than a century ago by Ludwig, and later by Soret, who observed it in electrolyte solutions [1, 2].

Over the years, the problem of thermal diffusion in polymer solutions has been addressed by various authors with varying success, but still today the understanding of the effect is only very rudimentary. Due to difficulties encountered with traditional experimental techniques, only a small and inconsistent experimental data base is available.

*To whom all correspondence should be addressed.

Debye and Bueche, [3] and later Langhammer, [4] employed a Clusius-Dickel fractionation tube, resulting in a difficult data analysis due to the presence of convective currents. A convection-free cell, which was heated from the top and cooled from the bottom, was employed by Emery and Drickamer, [5] by Hoffman and Zimm, [6] and by Whitmore [7]. Due to the macroscopic diffusion length on the order of 1 cm, equilibration times of several days are reported, making the experiments very time consuming and susceptible to perturbations, like weak residual convective currents.

Meyerhoff and Nachtigall [8] replaced the cumbersome concentration analysis of the final steady-state solute distribution by an optical beam deflection technique, utilizing the refractive index gradient that accompanies the concentration gradient. A state-of-the-art thermal diffusion cell based on laser beam deflection has been described by Kolodner et al. [9] for the measurement of the Soret coefficient of an ethanol/water mixture.

A completely different approach was chosen by Giddings and coworkers, [10] who utilized the Ludwig-Soret effect for thermal field flow fractionation (TFFF) inside a narrow flow channel with a strong temperature gradient applied perpendicular to the flow direction. For suitable polymer/solvent combinations, peak separation comparable to, or better than, size exclusion chromatography is obtained [11]. Selectivity, and thus fractionation, is introduced by the different molar mass dependence of the thermal diffusion coefficient D_T, and the translational diffusion coefficient D. Within the error limits of presently available experimental data, D_T may even be assumed to be independent of molar mass. By mathematically modeling the retention inside the flow channel, the Soret coefficient, $S_T = D_T/D$, can be extracted [12]. The method as a tool for the measurement of thermal diffusion coefficients is, however, complicated by the necessity for subtle corrections, like the temperature dependence of the viscosity due to the strong temperature gradients up to 5000 K/cm, or for nonlinear temperature profiles. Furthermore, only S_T is determined, and the more fundamental D_T can only be obtained if D is known from somewhere else.

Nearly all of the more recent experimental data have been measured by TFFF, and many interesting questions, like molar mass dependence, [13] temperature dependence, [14] or composition dependence in copolymers, [15] have been addressed.

Unfortunately, a comparison between the different techniques is restricted to very few cases, since nearly all the early experiments were done exclusively on polystyrene in toluene. Giddings et al. [12] have compared data for the thermal diffusion factor $\alpha = TD_T/D$, obtained by Taylor, Emery and Drickamer, Meyerhoff and Nachtigall, and in their own laboratory at different times. The differences are as high as several hundred percent, and there is not even an agreement between any two authors.

The phenomenological diffusion equations that can be derived from nonequilibrium thermodynamics contain the diffusion coefficients D and D_T as parameters, whose values cannot be determined from thermodynamical arguments. As, for example, for the specific heat, a microscopic theory is needed for a quantitative understanding of these diffusion coefficients. Schimpf and Giddings [13] tested available microscopic theories, which, however, had been developed

mainly for small molecules, against available experimental results. They included a theory based on statistical mechanics by Bearman, Kirkwood, and Fixmann, kinetic theories of Emery and Drickamer, of Ham, and of Khazanovich, a collision model of McNab and Meisen, and a radiation pressure theory of Gaeta. A detailed discussion of the various theories, including references to the original papers, can be found in reference 13. All above theories failed to predict essential experimental findings, like the correct molar mass dependence of D_T, or could not be tested, because required material parameters were not known.

Thus the currently available experimental results are still rather limited and inconsistent. Furthermore, despite being a very fundamental transport property, there is up to now no convincing microscopic theory for the thermal diffusion coefficient. This unsatisfactory situation is largely due to the experimental problems of getting reliable data within a reasonable time.

Recently a sensitive holographic technique known as forced Rayleigh scattering (FRS) has been successfully employed in our laboratory to investigate thermal diffusion in polymer solutions [16]. By writing an optical interference grating into a slightly absorbing sample a spatially periodic temperature distribution is created. Thermal diffusion is driven by the temperature gradients within this temperature grating, giving rise to a concentration grating superimposed upon the thermal one. By Bragg diffraction of a readout laser beam the formation and the decay of both the temperature and the concentration grating, in response to a pulsed excitation, can be measured. Three different diffusion coefficients—the thermal diffusivity D_{th}, the translational diffusion coefficient D, and the thermal diffusion coefficient D_T—are obtained, requiring neither external calibration nor absolute intensity measurement. Due to the micrometer diffusion lengths within the holographic grating, equilibration takes place on a millisecond time scale, as compared with many hours reported for the macroscopic diffusion cells. Contrary to conventional FRS, this technique does not require photochromic chain labeling.

THEORY

Transport properties such as mass diffusion or thermal diffusion, in systems not too far away from thermal equilibrium, are described within the framework on non-equilibrium thermodynamics. Starting with the concept of internal entropy production, dS_i/dt, a dissipation function Φ is defined, which is then expressed as a sum over products of flows, $\vec{J}_\alpha$, and generalized forces, $\vec{X}_\alpha$: [17]

$$\Phi = T\frac{dS_i}{dt} = \sum_\alpha \vec{J}_\alpha \vec{X}_\alpha \tag{1}$$

In a binary system, like a polymer solution, there is a flow of heat, $\vec{J}_q$, and a flow of matter, $\vec{J}_m$. According to Onsager, a linear relationship holds between the flows and the forces:

$$\vec{J}_\alpha = \sum_\beta L_{\alpha\beta}\vec{X}_\beta \tag{2}$$

The diagonal terms in Equation (2) describe the well-known laws of heat and mass diffusion, known as Fourier's law and Fick's law. Cross-coupling between temperature and concentration is introduced by the off-diagonal coefficients L_{qm}, which causes heat flow due to a concentration gradient (Dufour effect), and L_{mq}, which gives rise to thermal diffusion (Ludwig-Soret effect), the flow of matter within a temperature gradient [17].

Usually, Equation (2) is not employed for a mathematical description of experiments, but the so-called phenomenological diffusion equations. Since the Dufour-effect is not of importance in liquids—there is no noticeable coupling between concentration gradients and heat flux—the appropriate set of phenomenological diffusion equations to incorporate thermal diffusion into the description of non-isothermal polymer solutions are the heat equation and an extension of Fick's second law of diffusion: [9, 17]

$$\frac{\partial T}{\partial t} = D_{th}\vec{\nabla}^2 T + \frac{\dot{Q}}{\rho c_p} \tag{3}$$

$$\frac{\partial c}{\partial t} = D\vec{\nabla}^2 c + D_T c(1 - c)\vec{\nabla}^2 T \tag{4}$$

$\dot{Q}$ is the local heat production, ρ the density, c_p the specific heat, and c the concentration in weight fractions. The diffusion coefficients in above equations can be expressed by the Onsager coefficients, $L_{\alpha\beta}$, and both ways of describing the problem are equivalent [17].

As will be described in the experimental section, an optical interference grating is written into the sample by means of two laser beams which intersect under an angle θ. The resulting intensity distribution, $I_w(x, t)$, with the x-direction perpendicular to the optical axis and defined by the grating vector $\vec{q}$, is:

$$I_w(x, t) = I_{w,0}(t)(1 + \cos qx), \qquad q = \frac{4\pi}{\lambda_w} \sin \frac{\theta}{2} \tag{5}$$

For a description of the experiment, the one-dimensional form of Equation (3) is solved first, with the energy absorbed by the sample from the optical interference grating as source term, $\dot{Q}(x, t) = \alpha I_w(x, t)$. α is the absorption coefficient and $I_w(x, t)$ is defined by Equation (5). The spatial and temporal temperature distribution within the sample is then given by:

$$T(x, t) = T_0 + T_m(t) + T_t(t)\cos qx. \tag{6}$$

The ambient temperature T_0 and the mean sample temperature during exposure T_m are of no concern [16], since they correspond to $q = 0$ and do not contribute to the Bragg diffraction experiment with q given by Equation (5).

$$T_t(t) = \frac{\alpha I_{w,0}(t)}{\rho c_p} \frac{1}{D_{th} q^2} \tag{7}$$

is the amplitude of the thermal grating that both shows up in the signal and causes the buildup of the concentration grating. Since the thermal lifetime is about three orders of magnitude shorter than the lifetime of the concentration grating, the memory term in $T_t(t)$ is neglected, and the temperature grating is assumed to follow the optical grating without delay. A discussion of the mean sample temperature and the time dependence of the thermal grating can be found in reference 16. It will be seen later that the right hand side of Equation (7) will never be needed explicitly, since all signals will be normalized to the amplitude of the thermal grating.

Driven by the temperature gradients within the thermal grating, a concentration grating starts to build up, whose amplitude is obtained from the one-dimensional solution of Equation (4), with $T(x, t)$ according to Equation (6). The calculation is straightforward and only the essential steps will be sketched below.

In analogy to Equation (7) the dependence of the concentration on space and time is written as:

$$c(x, t) = c_0 + c_t(t)\cos qx. \tag{8}$$

where c_0 is the initial concentration of the homogeneous solution. Inserting Equations (7) and (8) into Equation (6) one obtains a linear differential equation for the time dependence of $c(t)$:

$$\frac{d}{dt}c_t(t) + q^2 Dc_t(t) = -q^2 D_T c_0(1 - c_0)T_t(t). \tag{9}$$

Here the approximation $c(1 - c) \approx c_0(1 - c_0)$ was made, which is always justified under experimental conditions where the relative changes of c stay well below 10^{-5} [16]. From linear response theory the solution of Equation (9) is obtained:

$$c_t(t) = -q^2 D_T c_0(1 - c_0)\int_{-\infty}^{t} dt' T_t(t')e^{-(t-t')/\tau}. \tag{10}$$

where $\tau = 1/Dq^2$ is the lifetime of the concentration grating and $e^{-t/\tau}$ is the response function, which is the solution of Equation (9) with the right hand side replaced by Dirac's δ-function, $\delta(t)$.

The sample is transparent at the readout wavelength and the readout laser beam is diffracted by a pure phase grating, which has contributions from both temperature and concentration. Again, the spatially constant terms are neglected, and the periodic modulation of the refractive index is:

$$n(x, t) - n_0 = \left[\frac{\partial n}{\partial T}T_t(t) + \frac{\partial n}{\partial c}c_t(t)\right]\cos qx. \tag{11}$$

where $\partial n/\partial T$ and $\partial n/\partial c$ are the respective contrast factors and have to be measured separately.

The heterodyne (η_{het}) and homodyne (η_{hom}) diffraction efficiencies [16, 18] for an excitation pulse lasting from t_1 to t_2, $T_t(t) = \delta T(h(t - t_1) - h(t - t_2))$, are

obtained after normalization to the pure thermal signal as:

$$\eta_{het}(t) \propto [h(t-t_1) - h(t-t_2)] - \frac{D_T}{D} c_0(1-c_0) \frac{\partial n/\partial c}{\partial n/\partial T} \left[h(t-t_1)\left(1 - e^{-(t-t_1)/\tau}\right) - h(t-t_2)\left(1 - e^{-(t-t_2)/\tau}\right) \right]$$

$$\eta_{hom} \propto \eta_{het}^2 \tag{12}$$

where $h(t)$ is the Heaviside step function, defined by $h(t < 0) = 0$, $h(t \geq 0) = 1$. D and D_T are extracted by fitting Equation (12) to the experimental data obtained from monodisperse polymer solutions, that can be described by a single relaxation time.

Two asymptotic cases are of special interest. Assuming $t_1 = 0$, $t_2 \to \infty$, and $t < t_2$, the saturation value for long pulses is:

$$\eta_{het}(t \to \infty) \propto 1 - \frac{D_T}{D} c_0(1-c_0) \frac{\partial n/\partial c}{\partial n/\partial T}, \tag{13}$$

and the short time expansion gives for the initial rise of the signal:

$$\eta_{het}(t \to 0) \propto 1 - tq^2 D_T c_0(1-c_0) \frac{\partial n/\partial c}{\partial n/\partial T}. \tag{14}$$

For the measurements reported here, $\partial n/\partial c$ and D_T are positive, whereas $\partial n/\partial T$ is negative. Thus, both the thermal and the concentration contribution to η_{het} are positive.

EXPERIMENTAL

The experimental setup shown in Figure 1 is an improved version of the basic setup described in reference 16. The vertically polarized line ($\lambda_w = 488$ nm) of an argon–ion laser (Spectra Physics 2020) is employed for writing. The beam is spatially filtered and expanded to about 10 mm in diameter, and then split into two beams of equal intensity, which are recombined within the sample.

For better stability the laser is operated without intracavity etalon. Since this reduces the coherence length to a few centimeters, a variable delay line is introduced to match the optical path lengths for maximum contrast within the grating.

A glass plate is used as a beam splitter to couple out a few percent of the two beams. At their point of intersection they create a secondary grating, which is projected by a microscope objective onto a video camera. Its output can be viewed on a monitor for correct beam alignment and contrast adjustment, and it can be

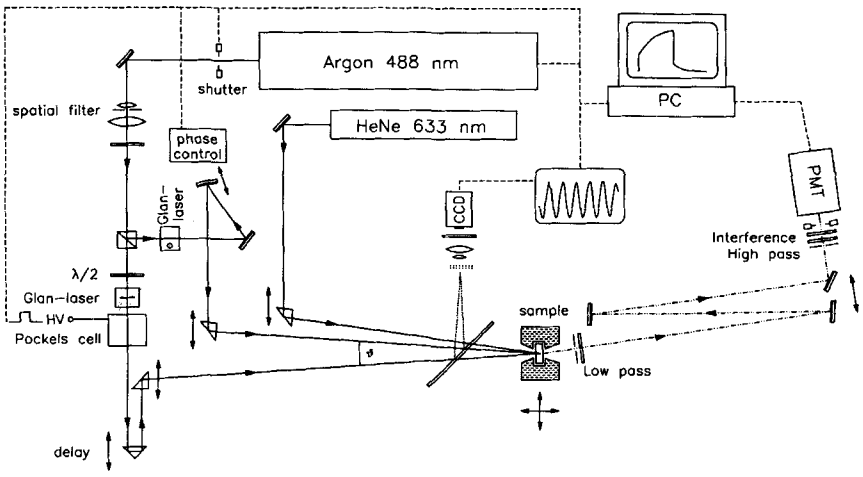

FIGURE 1 Experimental setup.

digitized and processed by a computer together with the image of a calibrated microscope reticle, which is placed at a position equivalent to the sample position. Since the video image is digitized within fractions of a second, problems arising from slow phase drifts are eliminated, and the fringe spacing of the grating is determined with a high accuracy ($\ll 1\%$), even for angles below 1 degree. The digitized intensity distribution within the grating and the projected scale of the reticle are shown in Figure 2.

Two different writing schemes have been employed. The first one is similar to that described in a previous publication [16]. In contrast to the setup shown in Figure 1, an electrooptic shutter is employed to switch both writing beams on and off. For this purpose, the half-wave plate and the first Glan-laser prism, which are used to polarize the laser beam horizontally, the Pockels cell, which is used to switch the polarization state between horizontal and vertical, and the second Glan-laser prism, which blocks the horizontally polarized beam, are placed *between* the spatial filter and the beam splitter.

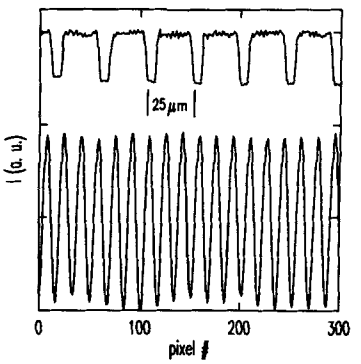

FIGURE 2 Digitized image of the intensity distribution within the interference grating (bottom), together with scale of calibrated microscope reticle (top). Here, the grating constant is 9.08 μm.

Alternatively the setup as shown in Figure 1 was used. When no voltage is applied to the Pockels cell, the polarization of the corresponding writing beam is horizontal, since it is rotated by the half-wave plate followed by the Glan laser prism. The polarization of the other writing beam is always vertical. Thus the two beams cannot interfere and the sample is evenly illuminated. When high voltage is applied to the Pockels cell, the polarization is rotated to vertical and an interference grating is formed at the sample position. The advantage of this technique is the constant average illumination of the sample during the on- and off-periods of the grating, eliminating all problems from transient heating effects that, though small, might be important for heterodyne detection [16].

The grating efficiency is measured by Bragg diffraction of a 35 mW He–Ne laser beam (NEC, $\lambda_r = 633$ nm). The diffracted beam is detected by a photo-multiplier tube in photon counting operation, connected to a multiple time-base counter card with 2-μs temporal resolution. Scattered light at the writing wavelength and fluorescence from the sample are removed by suitable filters, and the Rayleigh scattering background from the sample is reduced by narrowing the solid angle for detection with a 1-mm pinhole at a 2-m distance from the sample. To save space, mirrors are used to fold the optical path three times. The whole detection arm can be rotated as one rigid unit around a vertical axis that goes through the center of the sample, allowing easy adjustment of the correct Bragg angle.

The mirror mounted on the piezo actuator is used to separate the homodyne and the heterodyne signal components by applying a 180° phase shift to one of the writing beams during every other exposure. Averaging the sums and the differences of successive pairs of scans yields the homodyne and the heterodyne signals, respectively [16].

Sample cells with 1.0-mm and 0.2-mm optical path length were employed, and details for preparation of the samples and dust free filtering of the solutions can be found in reference 16.

For all experiments, polystyrene calibration standards (Polymer Standard Services, $M_w = 47{,}400$, 410,000, and 545,000 g/mol, $M_w/M_n = 1.03$–1.05) at concentrations between 1 g/L and 20 g/L, and high quality solvents (for chromatography) were used. The solutions were slightly colored with quinizarin (1,4-dihydroxyanthraquinone, Aldrich) to adjust the optical density between 1 (1-mm cell) and 2 (0.2-mm cell) for 1-cm optical path length. The temperature was 24°C for the measurements shown in Figures 6 and 7, and approximately 22°C in all other cases.

The contrast factors $\partial n/\partial c$ and $\partial n/\partial T$ were measured with a scanning Michelson interferometer which will be described in detail elsewhere [19].

RESULTS AND DISCUSSION

First experiments were done with polystyrene in ethyl acetate in a cell with an optical path length of 1 mm, and the data were evaluated by a nonlinear-least-square fit [20] of Equation (12) to the homodyne signal.

Some results are reported in a previous publication, [16] where it could be shown that Equation (12) provides a good description of the effect. The diffusive nature of the observed process could be proved by a variation of the fringe spacing

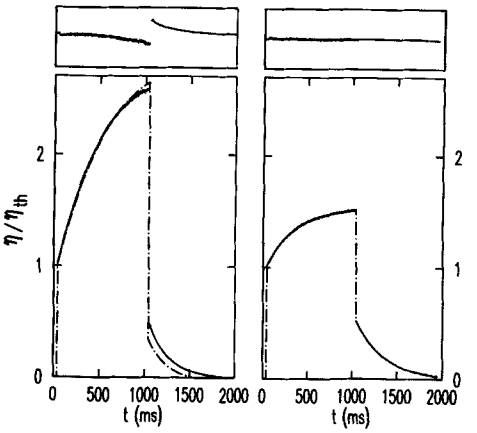

FIGURE 3 Influence of convection: normalized diffraction efficiencies with fit (dashed line) of Equation 12. Top: residues plotted on same scale; sample: PS (424,000 g/mol)/toluene, $c \approx 5$ g/L; left: 200 mW/cm^2, 1-mm cell, homodyne detection; right: 20 mW/cm^2, 0.2-mm cell, heterodyne detection.

of the grating, confirming the required proportionality between the relaxation time and the square of the diffusion length. Both for D and D_T, no dependence on the scattering vector was found in the q-range between 1,760 cm^{-1} and 12,320 cm^{-1}, corresponding to fringe spacings from 35.7 μm to 5.1 μm. Within experimental error, the translational diffusion coefficient of polystyrene in ethyl acetate agreed reasonably well with the one measured by photon correlation spectroscopy.

The time-dependent diffraction efficiencies of a typical experiment can be seen at the right hand side of Figure 3. After the optical interference grating is turned on at t = 50 ms, there is a fast rise of the diffraction efficiency due to the thermal grating, which is not time resolved in Figure 3. In reference 16, the thermal diffusivity, D_{th} has been determined from a time resolved measurement of the pure thermal process. Between t = 50 ms and t = 1,050 ms, the formation of the concentration grating is observed. At t = 1,050 ms, the optical grating is switched off and the thermal grating decays almost instantaneously. For longer times, the diffusive decay of the concentration grating can be seen. From the time dependence of the concentration grating the translational diffusion coefficient D, and from the amplitude ratio of both contributions the Soret coefficient $S_T = D_T/D$ are obtained. According to Equation (14), D_T can also be determined from the initial slope of the concentration grating, which will be discussed later.

Care has to be taken to avoid convection due to the rise of the mean sample temperature by some fractions of a degree within the illuminated spot. With 1-mm cells, low-viscosity solvents, and power levels around 100 mW/cm^2, convection can hardly be suppressed completely. Especially during prolonged exposure some signal distortion could be observed. By adding some μm-sized polyethylene particles, whose motion can be tracked with a microscope and a video camera, the onset of convection could be observed visually. Two measures turned out to be quite efficient for avoiding convection problems: a reduction of the cell thickness to 0.2 mm, and a precise alignment of both grating and sample in a way, that any residual convective currents within the illuminated spot are exactly parallel to

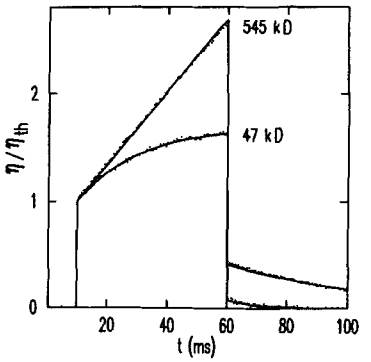

FIGURE 4 Normalized homodyne diffraction efficiencies of PS/ethyl acetate with fit of Equation 12. $c \approx 6$ g/L, $M_w = 47{,}400$ g/mol and $M_w = 545{,}000$ g/mol.

the grating. Such convection parallel to the grating, which is perpendicular to the direction of $\vec{q}$, is of no influence, due to the translational symmetry along the vertical direction.

Unfortunately, the convection problem had not been identified during the first experiments, and some of the measurements may suffer from it. The deviations of about 10% in the D_T data from reference 16 measured at different q-values, are probably caused by this problem.

The effect of convection is shown in Figure 3. The curve on the left hand side was measured with a 1-mm cell with an intensity of about 200 mW/cm^2. The fit of Equation (12) is rather poor, as can be seen from the systematic deviation of the residues. Contrary, the measurement with the 0.2-mm cell and a writing intensity of 20 mW/cm^2 is almost perfectly described by Equation (12), and a further reduction of the laser power gave no change.

It follows from Equation (14), that the initial rise of the signal only depends on D_T, but not on D. Since all other quantities are known, D_T can thus be obtained from the response to short excitation pulses without the need for long exposure times. This is of advantage, if the thermal load needs to be kept as low as possible. It has been observed that, even with thick sample cells, convection needs some time to develop, and it is almost never a problem during the first 100 ms. Figure 4 shows results for two polystyrene samples of different molar mass, but identical concentration, in ethyl acetate. Because of its high diffusion coefficient, the sample with a molar mass of 47,400 g/mol nearly reaches saturation during the exposure time, whereas the sample with 545,000 g/mol is still not far beyond the initial linear regime. The initial slopes of the concentration signals agree within a few percent, indicating a molar mass independent thermal diffusion coefficient D_T, which is in agreement with the literature [13, 21].

With heterodyne detection, the signal is proportional to the amplitude of the refractive index grating, whereas with homodyne detection it is proportional to its square. Thus for weak signals heterodyne detection should be chosen because of its superior signal to noise ratio. Generally, the diffracted beam contains both homodyne and heterodyne contributions, which can be separated by a procedure described in the experimental section. As long as the signals are not too weak, the extraction of the homodyne part poses no problem.

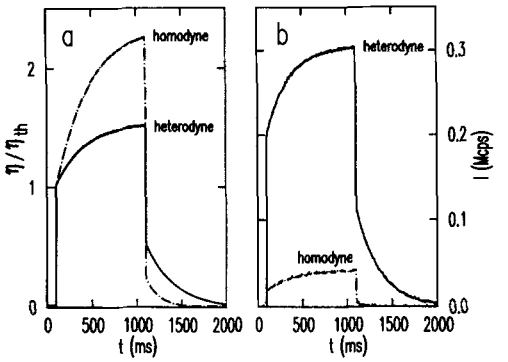

FIGURE 5 Homodyne and heterodyne signals of PS (424,000 g/mol)/toluene. a) $I \approx 100$ mW/cm^2, normalized to thermal signal; b) $I \approx 20$ mW/cm^2, not normalized.

The heterodyne signal may suffer from transient heating effects during exposure if thick cells and high intensities are employed. With thin cells, and by avoiding excessive laser power, satisfactory results could be obtained, and polarization switching with a constant average intensity on the sample eliminates the problem completely. Another complication comes from the unavoidable slow—on the time scale of minutes—phase drift of the optical interference grating which, at best, leads to a decrease of the heterodyne signal over time. In the worst case, the heterodyne signal may even be averaged away completely. By employing an active phase stabilization, where the phase between the diffracted beam and the reference wave is constantly monitored and adjusted between exposures, the heterodyne signal can be averaged over an arbitrary time. Details of this procedure will be described in a forthcoming paper [22].

A good local oscillator for the reference wave is provided by dust particles or small scratches on the exit window of the cell. By horizontal and vertical translation it is not very difficult to find a suitable spot. Practically, the incoherent contribution to the background can be reduced to less than 10 percent.

Figure 5 shows a comparison between homodyne and heterodyne detection. In Figure 5a both signals are normalized to the thermal contribution, and their signal-to-noise ratios during the excitation pulse are approximately the same. The heterodyne signal is already of advantage during the free decay of the concentration grating after the laser pulse.

In Figure 5b the laser intensity was reduced, and the curves are plotted without normalization. The advantage of heterodyne detection is evident, especially the heterodyne decay curve of the concentration grating, which still shows a good signal-to-noise level, whereas its homodyne counterpart nearly completely vanishes in the noise.

To demonstrate the performance of the method, Figures 6 and 7 show the concentration dependence of D, S_T, and D_T for polystyrene in toluene. The measured translational diffusion coefficients are almost identical to the ones obtained by photon correlation spectroscopy (PCS), which are also plotted in Figure 7. Especially for low concentrations, the values are almost identical. Whether the slight deviation at higher concentrations is real or an artifact cannot

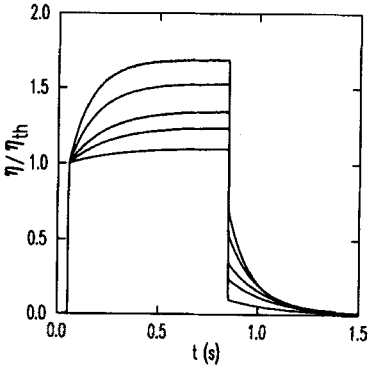

FIGURE 6 Normalized heterodyne diffraction efficiencies of PS (424,000 g/mol)/toluene. Concentrations 1.13, 3.11, 4.95, 9.93, and 15.8 g/L.

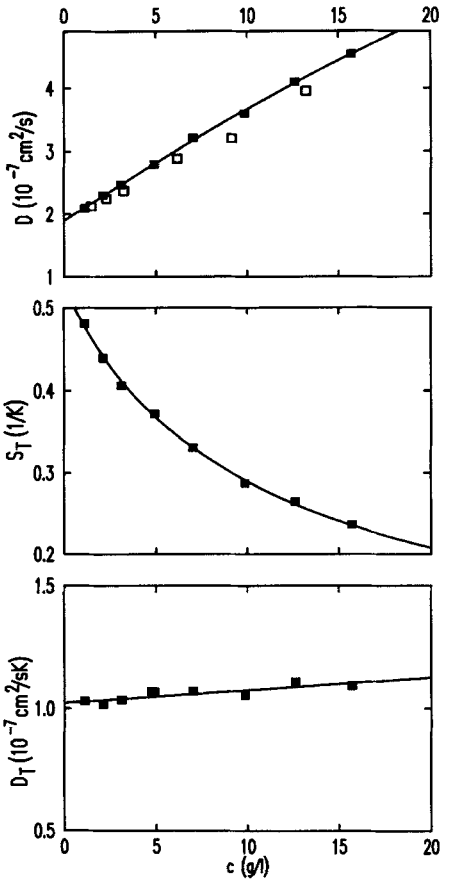

FIGURE 7 Concentration dependence of D, S_T, and D_T for PS (424,000 g/mol)/toluene. Open symbols: translational diffusion coefficients measured by photon correlation spectroscopy.

be judged from presently available data. The time needed for the FRS and the PCS measurements was about the same.

The thermal diffusion coefficient D_T shows a very slight increase with concentration. The extrapolated value for zero concentration is almost identical to the one found by Meyerhoff and Nachtigall [21] at a somewhat different temperature (20°C). They reported, however, a slight decrease with increasing concentration.

The values used for the contrast factors are $\partial n/\partial c = 0.1096$ mL/g and $\partial n/\partial T = -5.62 \times 10^{-4}$ K^{-1}, and no noticeable concentration dependence was observed at the low concentrations used in the experiments. The fringe spacing of the grating was 14.40 μm.

CONCLUSION

Forced Rayleigh scattering provides a sensitive tool for the investigation of thermal diffusion in polymer solutions. Whereas traditional diffusion cell techniques require long equilibration times, the diffusion length is now reduced to micrometers, resulting in very short sub-second response times. A simple mathematical model is sufficient for an excellent phenomenological description of the observed effect. Three different diffusion coefficients, D_{th}, D, and D_T are obtained from a single experiment, and no chemical modification of the polymer chains is required. By an improved optical setup, disturbing convection is virtually eliminated, and active phase tracking allows the utilization of the heterodyne signal with its superior signal to noise characteristic for weak signals.

Acknowledgments

The authors thank the polymer analytical group of the institute for continual support, especially B. Müller for measuring the contrast factors, and C. Rosenauer for the photon correlation spectroscopy measurements.

References

1. C. Ludwig, *Sitzber. Akad. Wiss. Wien Math.-naturw. Kl.*, **20**, 539 (1856).
2. C. Soret, *Arch. Geneve*, **3**, 48 (1879).
3. P. Debye and A. M. Bueche, in H. A. Robinson, ed., *High Polymer Physics* (Chemical Publishing, Brooklyn, 1948).
4. G. H. Langhammer, H. Pfennig, and K. Quitzsch, *Z. Elektrochemie*, **62**, 458 (1958).
5. A. H. Emery and H. G. Drickamer, *J. Chem. Phys.*, **23**, 2252 (1959).
6. J. D. Hoffman and B. H. Zimm, *J. Polym. Sci.*, **15**, 405 (1955).
7. F. C. Whitmore, *J. Appl. Phys.*, **31**, 1858 (1960).
8. K. Nachtigall and G. Meyerhoff, *Makromol. Chem.*, **33**, 85 (1959).
9. P. Kolodner, H. Williams, and C. Moe, *J. Chem. Phys.*, **88**, 6512 (1988).
10. J. C. Giddings, M. E. Hovingh, and G. H. Thompson, *J. Phys. Chem.*, **74** 4291, (1970).
11. J. J. Gunderson and J. C. Giddings, *Anal. Chim. Acta*, **189**, 1 (1986).
12. J. C. Giddings, K. D. Caldwell, and M. N. Myers, *Macromolecules*, **9**, 106 (1976).
13. M. E. Schimpf and J. C. Giddings, *J. Polym. Sci.*, **B27**, 1317 (1989).
14. S. L. Brimhall, M. N. Myers, K. D. Caldwell, and J. C. Giddings, *J. Polym. Sci., Polym. Phys. Ed.*, **23**, 2443 (1985).

15. M. E. Schimpf and J. C. Giddings, *J. Polym. Sci., Part B, Polym. Phys. Ed.*, **28**, 2673 (1990).
16. W. Köhler, *J. Chem. Phys.*, **98**, 660 (1993).
17. H. J. V. Tyrrell, *Diffusion and Heat Flow in Liquids* (Butterworth, London, 1961).
18. H. J. Eichler, P. Guenther, and D. W. Pohl, *Laser-Induced Dynamic Gratings* (Springer, Berlin, 1986).
19. A. Becker, W. Köhler, and B. Müller, *Ber. Bunsenges. Phys. Chem.*, accepted.
20. H. Späth, *Algorithmen für Multivariable Ausgleichsmodelle* (Oldenburg, München, 1973).
21. G. Meyerhoff and K. Nachtigall, *J. Polym. Sci.*, **57**, 227 (1962).
22. W. Köhler, *J. Phys. Chem.*, submitted.